Investigation of Synthesizing MCM-41/ZSM-5 Composites

Limin Huang,[†] Wanping Guo,[†] Peng Deng,[†] Zhiyuan Xue,[‡] and Quanzhi Li*[,†]

Department of Chemistry, Fudan University, Shanghai 200433, PRC Center of Analysis and Measurement, Fudan University, Shanghai 200433, PRC

Received: March 11, 1999; In Final Form: September 12, 1999

MCM-41/ZSM-5 composites were prepared using a dual templating method through a process of two-step crystallization. Mesoporous MCM-41 was first synthesized using the self-assembling of surfactant cetyltrimethylammonium bromide and subsequently the amorphous wall of MCM-41 was recrystallized with a structure-directing agent tetrapropylammonium bromide, which was introduced into the MCM-41 wall through a pretreatment process. A solid to solid-phase transformation mechanism was presented for the recrystallization of MCM-41 framework. Two kinds of stable MCM-41/ZSM-5 composites can be synthesized during the course of recrystallization. Crystallized mesoporous MCM-41 containing only short-range ordered ZSM-5 structure was first synthesized in the early stage of the recrystallization. With the increase of recrystallization time, some discrete micron-sized ZSM-5 crystals were produced and firmly attached to the loose aggregates of crystallized MCM-41, and another kind of MCM-41/ZSM-5 composite containing interconnected mesopore and micropore was therefore obtained. Because of improved acidity and a 2-fold pore system, both MCM-41/ZSM-5 composites are more advantageous than amorphous MCM-41 and a mechanical mixture of MCM-41 and ZSM-5 in acid catalysis.

1. Introduction

Recently, much attention has been given to the potential uses of Al containing mesoporous molecular sieves as acid catalysts because of their tunable uniform mesostructures (20−300 Å).[1,2] However, the weak or medium strength of acidity arising from the amorphous character of mesoporous materials may greatly limit their extensive uses.[3−6] Microporous molecular sieves (pore diameter < 15 Å) such as zeolite Y, ZSM-5, and β, which have abundant uniform microporous structures and strong intrinsic acidities, have played important roles in acid catalysis. All excellent performances of these materials can be attributed to their crystallographic structures. Unfortunately, large molecules cannot react effectively over these microporous materials because of the limitation of their small pore sizes. Therefore, to upgrade the performances of mesoporous and microporous molecular sieves, great interest has been aroused to synthesize a new kind of composite material, which combines the advantages of these two kinds of molecular sieves. Up to now, only a few articles concerning this study have been published.[7−12] For example, Kloetstra et al.[7] prepared zeolite faujasite overgrown with a thin layer of mesoporous MCM-41, by successive synthesis of FAU and MCM-41 or by adding FAU crystals to MCM-41 synthesis gel. The composite MCM-41/FAU they made has shown good results in cracking of vacuum gasoil. Karlsson et al.[11] also prepared composite materials by simultaneous synthesis of MFI/MCM-41 phases using a two-template approach [$C_6H_{13}(CH_3)_3NBr$ and $C_{14}H_{29}(CH_3)_3NBr$] at optimized template concentrations and reaction temperatures.[11]

Because all the disadvantages of mesoporous materials are closely associated with their amorphous frameworks, one can imagine that, if the amorphous framework of MCM-41 is recrystallized using a MFI structure-directing agent tetrapropylammonium cations (TPA^+), a kind of MCM-41/ZSM-5 composites can probably be produced. However, it was found that, although treating calcined MCM-41 with a solution of tetrapropylammonium hydroxide at 170 °C produced surface tectosilicate structure at first, the mesostructure totally collapsed with further recrystallization.[8] The reason may lie in the severe conditions of high alkalinity and high temperature during the recrystallization. The MCM-41 framework was destroyed because the inorganic species tended to be dissociated from the mesostructure for ZSM-5 formation under such conditions. Evidently, the stability of MCM-41 mesostructure is quite essential during the recrystallization.

We have found that mesoporous MCM-41 can remain stable, both in its phase symmetry and structural regularity, for at least 10 days with the temperature no higher than 150 °C and pH no higher than 10.5. Under the circumstances, however, the posttreatment of calcined Al−MCM-41 (Si/Al =14) with 1 M TPABr did not produce the ZSM-5 phase. In this case, only a few TPA^+ cations were exchanged to the surface cationic positions of MCM-41 framework. As a result, the TPA^+ cations cannot effectively direct the recrystallization of MCM-41 because of the less strong interactions between TPA^+ cations and aluminosilicate. Likewise, Kloestra et al. successfully prepared mesoporous materials containing framework tectosilicate (PNA-1, 2) from TPA^+ ion-exchanged Al−MCM-41 and Al−HMS.[9] The recrystallization degrees of PNA-1,2 are low also because TPA^+ cations cannot fully direct the recrystallization of the mesoporous materials. Thus, a so-called pretreatment process was carried out by premixing inorganic sources with TPABr solution followed by a certain period of aging before they were added to a cetyltrimethylammonium bromide (CTAB) solution. Through this process, the strong interactions between TPA^+ cations and aluminosilicate precursors can be preserved with the formation of MCM-41 structure, and the

* Corresponding author. E-mail: qzli@fudan.edu.cn.
† Department of Chemistry.
‡ Center of Analysis and Measurement.

10.1021/jp990861y CCC: $19.00
Published on Web 03/09/2000

recrystallization of MCM-41 may be effectively guided under certain conditions.

The so-called pretreatment is an important procedure for synthesizing MCM-41/ZSM-5 composites. From the viewpoint of thermodynamically and kinetically driving forces in the gel system (SI, SS, II stands for the interaction between surfactant and inorganic species, among surfactants, and among inorganic species, respectively), the interaction order should be SI > SS > II to synthesize the mesoporous phase, whereas it should be OI > OO and II > OO for synthesizing microporous phase (O stands for structure-directing agent).[13] Therefore, if microporous ZSM-5 phase is crystallized on the basis of presynthesized mesoporous MCM-41 phase, the following relations should be satisfied: (1) SI > SS > II > OO and (2) OI > OO. It suggests that the addition of TPA^+ does not change the thermodynamically driving force order for synthesizing MCM-41 phase. In addition, it also indicates that the strong interaction between CTA^+ cation and aluminosilicate species (SI) and the strong interaction between TPA^+ cation and aluminosilicate species (OI) are important for the formation of MCM-41 and ZSM-5, respectively. Thus, there is a balance between SI and OI, which can be controlled by the time of so-called pretreatment process. If the pretreatment time is too long, the over-condensed inorganic species may carry less surface charge density, thus reducing its ability to combine electrostatically with CTA^+ ions, i.e. the interaction SI is reduced. As a result, no or less MCM-41 mesostructure can be finally produced. On the contrary, a short time of the pretreatment process is not sufficient for the presence of strong interaction of OI.

In this article, we propose a two-step crystallization process for synthesizing MCM-41/ZSM-5 composites. It involves (I) construction of MCM-41 mesostructure, (II) introduction of TPA^+ cations within the mesopore wall of MCM-41 through the so-called pretreatment process, and (III) recrystallization of the amorphous wall of MCM-41 directed by TPA^+ cations. In the process of the two-step crystallization, the mesoporous MCM-41 phase was first prepared during the first-step crystallization. In this step, the synthesis conditions such as temperature and alkalinity are beneficial to moving the aluminosilicate polymerization equilibrium for high conversion toward well-ordered MCM-41.[14−16] Meanwhile, because of the strong repulsion between CTA^+ and TPA^+, the positively charged TPA^+ cations with voluminous hydrocarbon side chains cannot possibly enter the micelle core or locate at the hydrophobic−hydrophilic region of the micelles to form a palisade layer. Thus, the TPA^+ cations are most likely introduced within the mesopore wall with the formation of MCM-41. In the process of the second-step crystallization (i.e. recrystallization), appropriate alkalinity and higher temperatures are controlled to boost the formation of ZSM-5 on the basis that the MCM-41 mesostructure can remain stable. When the mesostructure was recrystallized at a lower temperature of 100 °C during the second-step crystallization, no long-range ordered ZSM-5 structure could be detected from its X-ray diffraction (XRD) profile even after the recrystallization time of 20 days. At the lower temperature of 100 °C, the thermodynamic driving force of OI is so weak that the inorganic species cannot be rearranged flexibly because of the relatively strong bondage between the supramolecular assembly of CTAB and aluminosilicate. However, a recrystallization temperature higher than 150 °C easily caused the damage of MCM-41 mesostructure. Therefore, an appropriate recrystallization temperature between 100 °C and 150 °C was chosen. Besides temperature, the alkalinity is another key factor for the recrystallization process. Because the gradual polymerization of aluminosilicate species in alkaline media would cause the increase of pH in the reaction system, it is important to maintain the gel's pH to a relatively low value to prevent the mesostructure from collapsing. By repeatedly adding diluted acid during the recrystallization, the pH can be reduced to the region where the mesostructure can be stable. On the other hand, the additional anions can also be introduced into the micelle interface, weakening the electrostatic interaction between aluminosilicate and surfactant.[17] Under such recrystallization conditions, the amorphous aluminosilicate species can be further rearranged within the mesopore wall of MCM-41 for ZSM-5 formation.

According to considerations above, a two-step crystallization process was carried out in this article to prepare MCM-41/ZSM-5 composites. Powder XRD, Fourier transform infrared (FTIR), ^{29}Si and ^{27}Al magic-angle spinning (MAS) NMR, scanning electron microscopy (SEM), transmission electron microscopy (TEM), N_2 adsorption−desorption isotherms, ^{129}-Xe NMR and thermogravimetric (TG) analysis were used to characterize the products obtained at various stages of the two-step crystallization. A possible synthesis mechanism for this synthesis was also discussed.

2. Experimental Section

Synthesis. A typical synthesis process is described as follows.[18] TPABr solution (3.55 g TPABr dissolved in 9 mL deioned water) was first combined with 16 g water glass (7.4% Na_2O, 25.4% SiO_2, 67.2% H_2O by weight) and $NaAlO_2$ solution (0.36 g sodium aluminate dissolved in 9 mL water). The initial clear mixture quickly gelled and transformed to a viscous, opaque white suspension, which was stirred vigorously for 1−4 h. Then the suspension was added to 44 g of 9.9 wt % CTAB solution and the whole mixture was stirred for 1 h. The final gel composition with molar ratio is: $0.32Na_2O{:}SiO_2{:}0.0334Al_2O_3{:}0.16$CTAB:$0.2$TPABr:$55H_2O$. Finally, a two-step crystallization process was performed. The first-step crystallization was performed at 100 °C and pH 11 for 2 days and the second-step crystallization (i.e. recrystallization) was performed at 125 °C and pH 9.5 for 1−12 days. The pH was reduced by adding 50 wt % acetic acid. The solid product recovered by filtration was washed with deioned water, dried at ambient condition, and calcined at 540 °C in N_2 flow for 1 h followed by 5 h in air.

Characterization. XRD patterns were obtained with a Rigaku D/MAX-IIA diffractometer system equipped with Ni-filtered Cu Kα radiation. TEM was performed with a JEM-200CX transmission electron microscope operated at 200 KV. SEM was obtained with a HITACHI S-520. N_2 adsorption−desorption isotherms were measured with a Micromeritics ASAP 2010 system. The pore size distribution curve was determined from the desorption branch of the isotherm. Differential thermogravimetric (DTG) analysis was performed on a Rigaku PTC-10A thermal analyzer under a flowing argon atmosphere with a heating rate of 10 °C/min. ^{129}Xe NMR spectra were recorded on a Bruker MSL-300 spectrometer at 20 °C. A certain number of xenon gas (1×10^{21} Xe atoms/g) were sealed with a 400-mg sample in a rotating tube at liquid N_2 temperature before collecting the ^{129}Xe NMR spectra. The catalytic cracking activities of *n*-dodecane were performed on a pulse microreactor at 500 °C. H-form samples were prepared by ammonium exchange at 70 °C for 2 h followed by calcination at 550 °C for 6 h.

3. Results and Discussion

Synthesis and Characterization of MCM-41/ZSM-5 Composites. Figure 1 shows the XRD patterns for as-synthesized

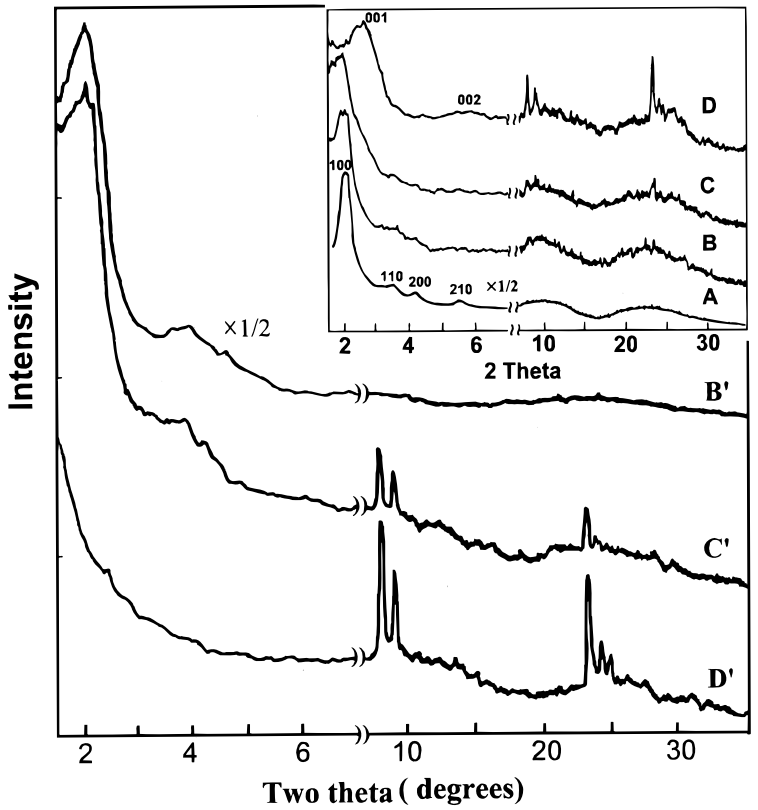

Figure 1. Powder XRD patterns of the products obtained at various stages of two-step crystallization. Calcined products: (B′) S1, (C′) S2, and (D′) S4. Inset, as-synthesized products: (A) S, (B) S1, (C) S2, and (D) S4.

TABLE 1: Physicochemical Properties of the Products Obtained at Various Stages of Two-step Crystallization

sample	crystallization time (d)	phase		d(100)[b] (nm)	pore size (wall thickness) (nm)	BET surface area (m^2/g)[c]
		mesopore	micropore			
		first-step crystallization (100 °C, pH = 11)				
S	2	H	none	4.18(4.01)	2.9(1.7)	870(0)
		second-step crystallization (125 °C, pH = 9.5)				
S1	4	DH	none	4.41(4.39)	3.1(2.2)	805(0)
S2	6	DH	ZSM-5	4.41(4.39)	3.1(2.2)	682(106)
S3	8	L	ZSM-5	3.48(−)	−	430(230)
S4	12	L	ZSM-5	3.27(−)	−	

[a] Abbreviations: H, hexagonal; DH, disordered hexagonal; L, lamellar. [b] The value inside the parentheses for d(100) is the value for calcined products. The wall thicknesses were calculated as: a_o− pore size ($a_o = 2 \times d(100)/\sqrt{3}$). [c] The value inside the parentheses for the BET surface area is the value for micropore calculated by t-plots and MP method.

(inset) and calcined samples obtained through the course of two-step crystallization. The physicochemical properties of the products are summarized in Table 1. In the process of the first-step crystallization, the XRD pattern (inset, Figure 1A) of sample S shows four distinct peaks indexable as (100), (110), (200), and (210) reflections, which is characteristic of long-range ordered hexagonal MCM-41. It indicates that when inorganic species was premixed with TPA^+ cations during the pretreatment, the electrostatic interactions between inorganic species and TPA^+ cation had no negative effect on preparing the hexagonal MCM-41 phase. Subsequently, the second-step crystallization (i.e. so-called recrystallization) was performed. For the product recrystallized for 4 d (sample S1), Figure 1B shows that the (100) diffraction peak broadens and the (110) and (200) diffraction peaks become indiscernible, indicating that sample S1 has a less ordered hexagonal mesostructure compared with sample S. In addition, Figure 1B shows no diffraction peaks corresponding to long-range ordered ZSM-5 in the high 2θ range. However, different from sample S, the FTIR spectroscopy of sample S1 (Figure 2) presents a broad but distinct vibration band at 550−560 cm^{-1}, which has been assigned to the asymmetric stretching mode of five-membered ring blocks

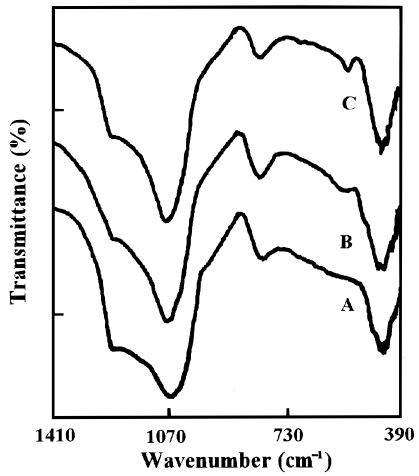

Figure 2. IR spectra of calcined samples (A) S, (B) S1, and (C) S3.

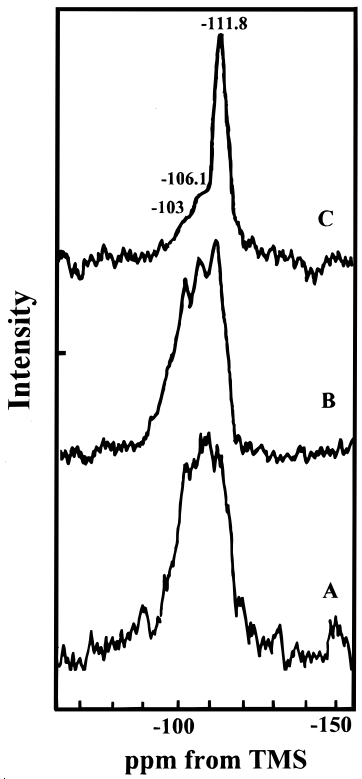

Figure 3. ^{29}Si NMR spectra of calcined samples (A) S1, (B) S2, and (C) S3.

(D5R) presented in the ZSM-5 structure. Thus, it can be deduced that only the short-range ordered ZSM-5 structure is in sample S1. While recrystallized for 6 d (sample S2), Figure 1C shows five small and broad diffraction peaks characteristic of ZSM-5 in the 2θ range of 8−25°, whose intensities increase a little after calcination at 550 °C (Figure 1C′). Meanwhile, the hexagonal mesostructure of sample S2 is still preserved, although the corresponding diffraction peak (100) becomes much broader and of lower intensity. Besides, a shoulder peak appears at the 2θ angle of ∼3°, which can be assigned to a thermally unstable phase (lamellar) because it disappeared with calcination (Figure 1C and 1C′). Moreover, Table 1 shows that both sample S1 and S2 have little mesopore shrinkage (∼0.5%) after calcination at 550 °C, representing the high degree of polymerization of aluminosilicate in the mesoporous frameworks. With the further increase of recrystallization time, the XRD results of samples S3 and S4 show that not only the crystallinities of their ZSM-5 phase increase further, but their mesostructural symmetries also greatly change. The symmetries are changed from hexagonal to lamellar (Figure 1D), which is structurally unstable under calcination (Figure 1D′).

Further characterization of the corresponding samples was done by ^{29}Si MAS NMR. The data are shown in Figure 3. Figure 3A shows three splitting peaks at −103 ppm, −106.1 ppm, and −111.8 ppm for sample S1, which is quite different from those for amorphous MCM-41.[1] In general, the peaks at −106.1 ppm can be assigned to the Si(0Al) units in amorphous MCM-41 framework, whereas the highest chemical shift at −111.8 ppm can be assigned to the crystallographically oriented Si−O−Si bonds or the crystalline Si(0Al) units. So, the peaks at −103 ppm and −111.8 ppm are attributed to the Si(1Al) and Si(0Al) units presented in ZSM-5, respectively. Figure 3A also shows a lower signal/noise ratio than Figure 3B or 3C (more scanning is needed to obtain an optimum spectrum for sample S1). It may suggest that although there are some crystal units in sample S1, the arrangement of Si−O−Si(Al) bonds is not as regular as that in ZSM-5. In other words, only short-range ordered structures with characteristics of ZSM-5 are produced in sample S1, which is in good agreement with the XRD and IR results above. As for sample S2 (Figure 3B), the peak intensity at −111.8 ppm increases, whereas the peak intensity at −106.1 ppm decreases. And the intensity of peak at −106.1 ppm greatly decreases with further recrystallization for sample S3 (Figure 3C), representing the increase of ZSM-5 crystal units with the increase of recrystallization time. Therefore, according to the characterization results of XRD, IR, and ^{29}Si NMR, phase transformations during the recrystallization proceed as follows: MCM-41 (long-range order) → MCM-41 (short-range order) + ZSM-5 (short-range order) → MCM-41 (short-range order) + ZSM-5 (long-range order) → lamella + ZSM-5 (long-range order).

The SEM images in Figure 4 show the morphologic changes of the samples during the recrystallization. Figure 4A shows only wormlike particles with some protrusions on the surface for sample S1, and no other phases can be observed. With further recrystallization, the SEM of sample S2 (Figure 4B) shows that the large wormlike particles transform to a great number of fine rodlike particles, which tend to form loose aggregates. Besides, a few discrete micron-sized particles, which are assumed to be ZSM-5 crystals, are closely attached to the loose aggregates (see the black arrowhead). As for sample S4, Figure 4C also presents loose aggregates formed by a greater number of fine rodlike particles with size of 0.1 × 0.2 μm, in which more micron-sized ZSM-5 crystals are embedded (see the black arrowhead). Moreover, every ZSM-5 crystal is attached to the fine rodlike particles, and no intergrowth or agglomeration is observed for the ZSM-5 crystals.

The morphology of the samples can also be observed from the TEM images presented in Figure 5. The images indicate that the channel of mesophase is changed from ordered hexagonal arrays for sample S (Figure 5A) to disordered, hexagonal-like packing for sample S1 or S2 during the recrystallization (Figure 5B and 5C). It is consistent with the XRD results showing the decrease of the long-range ordered hexagonal symmetries of the mesophase. In addition, in Figure 5C, one can observe beardlike structures attached on the surface of the disordered mesostructures, which are supposed to arise from the collapsed lamellar structures. Also, the deep color region in the beardlike structures may correspond to nanometer-sized ZSM-5 entities. Therefore, the disordered mesostructures of samples S1 and S2 probably result from the recrystallization of MCM-41 framework, which are quite different from the disordered channels in mesoporous material HMS or KIT.[19,20]

Although the mesostructures are disordered for samples S1 and S2, the results of N_2 adsorption indicate that they have uniform mesopores in pore size. The N_2 adsorption−desorption isotherm along with the pore size distribution calculated by Barrett-Joyner-Halenda method for sample S2 is presented in Figure 6. It exhibits a hysteresis loop in the region of P/P_o = 0.15−0.4 indicating a framework-confined mesopore with the pore size of 3.1 nm. It is remarkable that the mesostructures of sample S2, although disordered, are as uniform in pore size as those in sample S with highly ordered hexagonal mesostructures (based on the full width at half-maximum for the pore size distribution curve). In the region of P/P_o = 0.4 to 1.0, there is a hysteresis loop with the general form of type B.[21] It indicates that besides the disordered mesostructures, there are slit-shaped pores contributed by the beardlike structures in sample S2 (see Figure 5C). Because the beardlike structures probably arise from

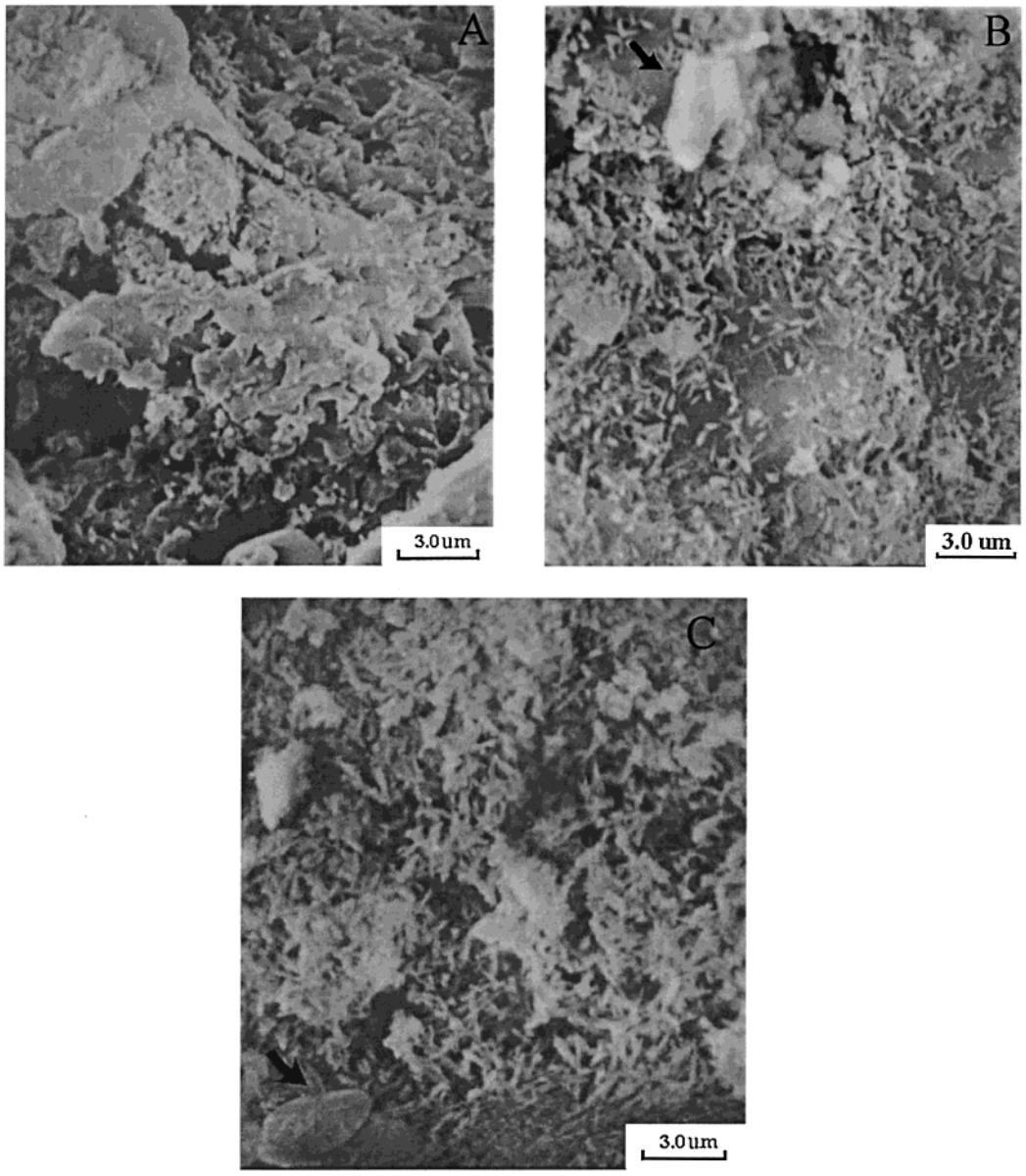

Figure 4. Representative SEM images of calcined samples (A) S1, (B) S2, and (C) S4.

the collapsed lamellar structures, the corresponding sides are rarely exactly parallel, and some of them can touch their neighbors so as to produce wedge-shaped pores. In addition, the collapsed lamellar structures may be nonrigid, so that the slit-width increases during adsorption and decreases during desorption. Therefore, the beardlike structures in sample S2 contribute to the formation of the type B hysteresis loop in Figure 6. In addition, the Brunauer-Emmett-Teller specific surface area for sample S2 is 682 m^2/g, of which 106 m^2/g is contributed by the micropore calculated with *t*-plots and MP method.[22,23] However, the micropore volume is zero for sample S1, showing that the short-range ordered ZSM-5 units make no or less contribution to the micropore volume (see Table 1).

As shown in Figure 4, each ZSM-5 crystal is attached to fine rodlike particles for sample S2. Also, the close contact between ZSM-5 phase and mesophase makes their pore structures highly interconnected, as can be proven by the ^{129}Xe NMR spectra in Figure 7. A mechanical mixture of MCM-41 and ZSM-5 phases, which has the same ZSM-5 content as sample S2, was used as a reference.[24] Both ^{129}Xe NMR spectra were collected at the same xenon adsorption capacity (1×10^{21} Xe atoms/g) and the same xenon equilibrium pressure. For the reference, the micropore of ZSM-5 and the mesopore of MCM-41 are totally independent. Figure 7B shows that there are three chemical shifts at 174.0, 84.6, and 0 ppm, corresponding to the xenon adsorbed in the microporous channel of ZSM-5, the mesoporous channel of MCM-41, and nonadsorbed xenon in the gas phase, respectively.[25,26] However, the ^{129}Xe NMR spectrum of sample S2 is quite different. In Figure 7A, one can see that the peak at 90.1 ppm is higher than that at 84.6 ppm and the peak shape becomes broadened and unsymmetrical, whereas the peak at 159.4 ppm is lower than that at 174.0 ppm and the peak shape becomes sharpened. The result is probably due to the existence of interconnected pores between micropore and mesopore for sample S2. When adsorbed, xenon molecules can be rapidly exchanged between the micropore and mesopore, thus resulting in one higher average chemical shift at 90.1 ppm and one lower chemical shift at 159.4 ppm. Therefore, the results of ^{129}Xe NMR well prove the interconnection between the micropore and mesopore for sample S2.

Synthesis Mechanism of MCM-41/ZSM-5 Composites. Through a so-called pretreatment process, it is found that the amorphous wall of MCM-41 can be recrystallized under the condition of 125 °C and pH 9.5 where the mesostructures can

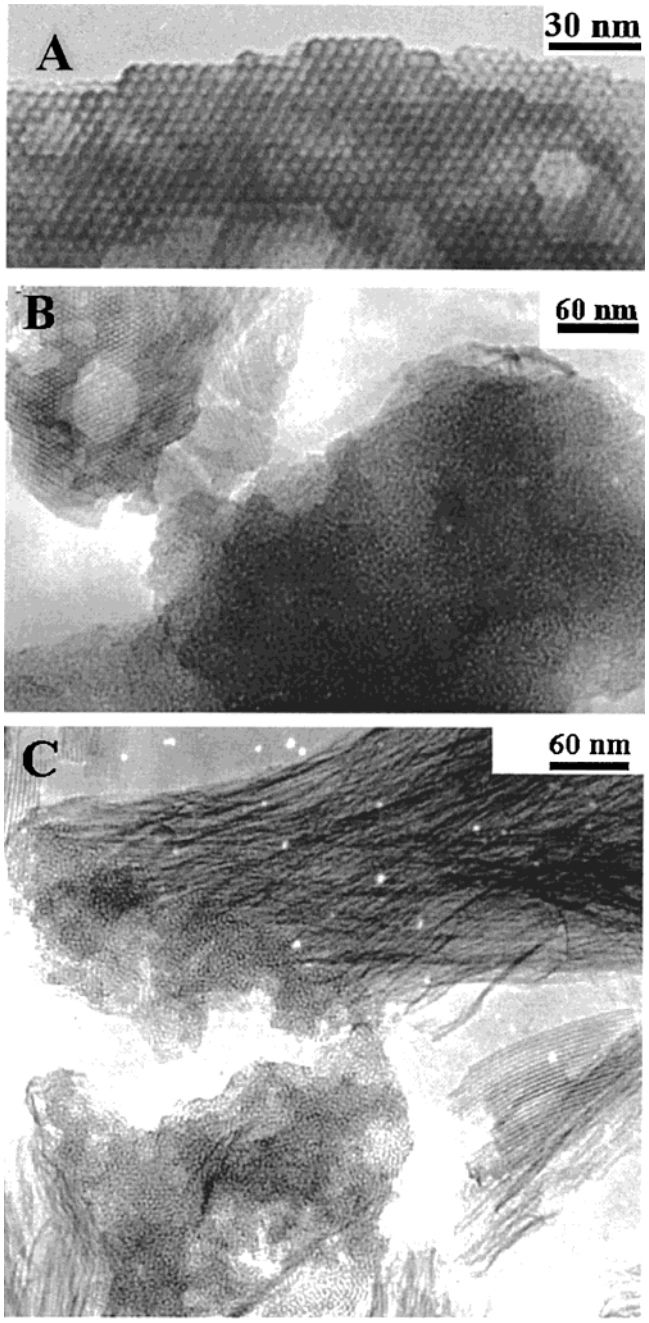

Figure 5. Representative TEM images of calcined samples (A) S, (B) S1, and (C) S2.

keep stable. It suggests that the recrystallization proceeds within the mesopore wall through a solid to solid-phase transformation, instead of a dissolution−crystallization mechanism. The following evidence further supports this suggestion. First, the XRD results in Figure 1 show that the MCM-41 mesostructure is not dissociated with the formation of ZSM-5, although its symmetry is changed from hexagonal to disordered hexagonal and finally to lamellar. A little increase in mesopore wall thickness from 1.7 to 2.2 nm during the recrystallization also indicates no dissolution of aluminosilicate from the MCM-41 wall (see Table 1). Second, the DTG curves for samples S2 and S4 are similar to those for hexagonal MCM-41 and lamellar mesophase, respectively. The desorption peaks for TPABr become so diffused that they can be covered up by CTAB desorption peaks. In addition, the total weight loss of organic species occluded in the product channel remains constant at 44−45 wt %. It can be imagined that, if the mesostructure of MCM-41 was dissociated

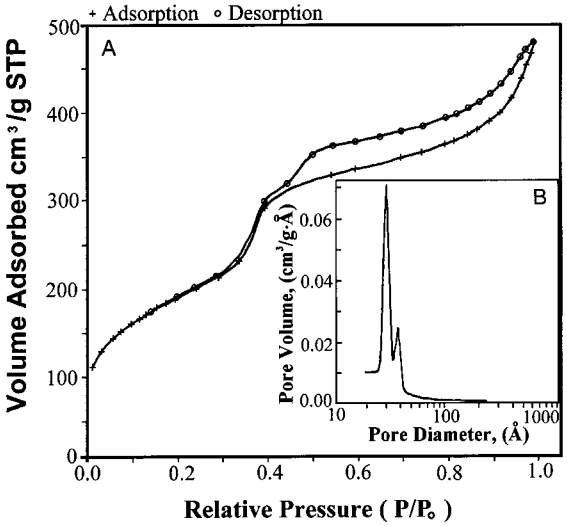

Figure 6. (A) Nitrogen adsorption−desorption isotherm and (B) BJH pore size distribution curve for calcined sample S2.

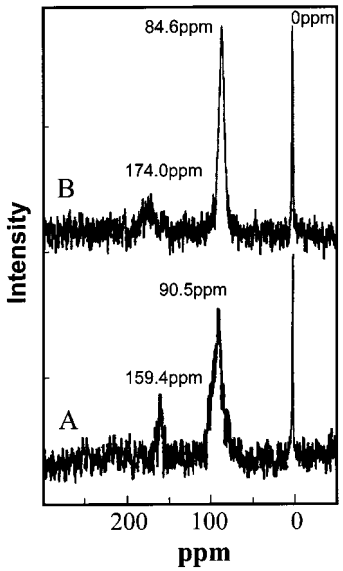

Figure 7. ^{129}Xe NMR spectra for (A) sample S2 and (B) mixture of MCM-41 and ZSM-5.

during the recrystallization, the surfactant aggregate would be broken up into many single CTAB molecules, which would be finally encapsulated within ZSM-5 channels or would enter the liquid phase and subsequently be washed away during collecting products. As a result, the decomposition peaks of CTAB included in ZSM-5 channels would be quite different from those of CTAB included in hexagonal or lamellar M41S,[27] and the total weight loss in TG curves would decrease because of the loss of CTAB molecules. Thus, the DTG results show that the mesostructures do not collapse with the recrystallization of MCM-41 framework. Moreover, the ^{27}Al NMR results indicate that all Al atoms mainly take the form of framework tetrahedral coordination and the SiO_2/Al_2O_3 ratios of the samples also remain as approximately 28 during the recrystallization. Therefore, according to all information above, a solid to solid-phase transformation mechanism can be put forward for the recrystallization of MCM-41 framework.

When the recrystallization proceeds, some additional bond strains are produced in the amorphous wall of MCM-41, resulting in the symmetric changes of the mesoporous phase. A brief scheme is shown in Figure 8. Because of the structure-directing role of TPA^+ cations, the crystallographic orientations

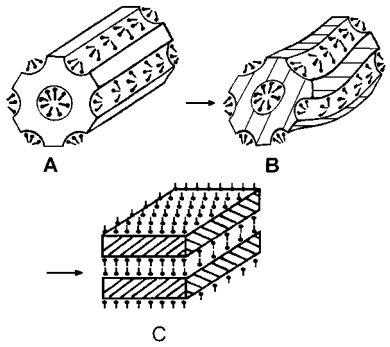

Figure 8. Schematic model for the structural transformation during the recrystallization: (A) hexagonal mesoporous, (B) disordered mesoporous, and (C) lamellar. □, amorphous; ///, crystallized.

of Si−O−Si (Al) bonds take place in the mesopore wall of MCM-41. Initially, the bond orientations make hexagonal MCM-41 mesostructure become disordered instead of structural collapse (Figure 8B). With the further recrystallization, more strong bond strains are produced in the framework of MCM-41, which can be greatly released by the phase transformation from disordered MCM-41 to lamellar mesophase with less curvature (Figure 8C). Moreover, the lamellar phase may be twisted further and folded to produce ZSM-5 entities with the increase of recrystallization time.

In conclusion, two kinds of MCM-41/ZSM-5 composites are obtained during the recrystallization of MCM-41 framework, according to whether ZSM-5 crystals have been produced and separated from the mesostructure. At the initial stage of recrystallization, the product is a crystallized MCM-41 phase containing only short-range ordered ZSM-5 structure. With further recrystallization, the MCM-41 mesostructure cannot sustain more local bond strains and some ZSM-5 crystals are separated from the mesoporous framework, producing another kind of MCM-41/ZSM-5 composite. In which, not only every ZSM-5 crystal is firmly attached to loose aggregates of crystallized MCM-41, but also their mesopore and micropore are highly interconnected. Because of the thin wall thickness of MCM-41 (<2 nm), it is difficult for nanometer-sized ZSM-5 to remain in the mesopore wall while preserving the stability of the mesostructure. However, the mesoporous materials with thicker walls may effectively sustain more local bond strains and produce nanocrystals in the mesopore walls.[28]

The MCM-41/ZSM-5 composites have shown very interesting results in cracking reactions. For sample S1, the mesoporous material containing only short-range ordered ZSM-5 shows improved acidity and cracking activities. For instance, the cracking activity of *n*-dodecane at 500 °C is 25% over H-form sample S1, compared with 9% over H-form MCM-41 with the same Si/Al ratio of 14. In addition, the bimodal pore structure in sample S2 has a positive effect on improving its reactivity. Its cracking activity of *n*-dodecane shows an increase by approximately 9% in comparison with the mechanical mixture of MCM-41 and ZSM-5 as the reference. It indicates that the interconnection of micropore and mesopore in sample S2 most likely facilitates the access of reactant molecules to acidic centers in the framework to upgrade its cracking performances.

4. Conclusions

In this article, we have successfully developed a two-step crystallization process using dual templates. Through the pretreatment of inorganic species and TPA^+ cations, the amorphous framework of MCM-41 can be recrystallized, producing two kinds of MCM-41/ZSM-5 composites. Moreover, the idea of this synthesis can be expanded to obtain other composite materials. More family members of the new composites with dual pore system are currently under development.[29]

Acknowledgment. Financial support from the National Natural Science Foundation of China (grant 29733070) is gratefully acknowledged.

Supporting Information Available: ^{27}Al NMR spectra of calcined samples, DTG curves of products of two-step crystallization, and cracking activities of alkanes over composite materials. This material is available free of charge via the Internet at http://pubs.acs.org.

References and Notes

(1) Beck, J. S.; Vartuli, C.; Roth, W. J.; Leonowicz, M. E.; Kresge, C. T.; Schmitt, K. D.; Chu, C. T−W.; Olson, D. H.; Sheppard, E. W.; McCullen, S. B.; Higgins, J. B.; Schlenker, J. L. *J. Am. Chem. Soc.* **1992**, *114*, 10834.

(2) Zhao, D.; Feng, J.; Huo, Q.; Melosh, N.; Fredrickson, G. H.; Chmelka, B. F.; Stucky, G. D. *Science* **1998**, *279*, 548.

(3) Davis, M. E. *Nature* **1993**, *364*, 391.

(4) Sayari, A. *Chem. Mater.* **1996**, *8*, 1840.

(5) Corma, A.; Fornes, V.; Navarro, M. T.; Perez-Pariente, J. *J. Catal.* **1994**, *148*, 569.

(6) Branton, P. J.; Hall, P. G.; Sing, K. S. W.; Reichert, H.; Schuth, F.; Unger, K. K. *J. Chem. Soc., Faraday Trans.* **1994**, *90*, 19, 2965.

(7) Kloetstra, K. R.; Zandbergen, H. W.; Jansen, J. C.; van Bekkum, H. *Microporous Mater.* **1996**, *6*, 287.

(8) Kloetstra, K. R.; Jansen, J. C.; van Bekkum, H. *Prepr.−Am. Chem. Soc., Div. Pet. Chem.* **1996**, *41*, 2, 412.

(9) Kloetstra, K. R.; van Bekkum, H.; Jansen, J. C. *J. Chem. Soc., Chem. Commun*. **1997**, 2281.

(10) Karlsson, A.; Stocker, M.; Schmidt, R. In *Proceedings of the 12th International Zeolite Conference*; MRS: Warrendale, PA, 1999; Vol. 1, p 713.

(11) Karlsson, A.; Stocker, M.; Schmidt, R. *Microporous Mesoporous Mater.* **1999**, *27*, 181.

(12) Huang, L.; Li, Q. In *Proceedings of the 12th International Zeolite Conference*; MRS: Warrendale, PA, 1999; Vol. 1, p 707.

(13) Stucky, G. D.; Huo, Q. S.; Firouzi, A.; Chmelka, B. F.; Schacht, S.; Voigt-Martin, I. G.; Schuth, F. *Progress in Zeolite and Microporous Materials*; *Studies in Surface Science and Catalysis*; Chon, H., Ihm, S.-K., Uh, Y. S., Eds.; Elsevier: Amsterdam, 1997; Vol. 105, Part A, p 3.

(14) Coustel, N.; Di Renzo, F.; Fajula, F. *J. Chem. Soc., Chem. Commun*. **1994**, 967.

(15) Ryoo, R.; Kim, J. M. *J. Chem. Soc., Chem. Commun*. **1995**, 711.

(16) Edler, K. J.; White, J. W. *Chem. Mater.* **1997**, *9*, 1226.

(17) Ryoo, R.; Jun, S. *J. Phys. Chem. B* **1997**, *101*, 317.

(18) Huang, L.; Chen, H.; Li, Q. Chinese Pat. Appl. 981109349, 1999.

(19) Bagshaw, S. A.; Prouzet, E.; Pinnavaia, T. J. *Science* **1995**, *269*, 1242.

(20) Ryoo, R.; Kim, J. M.; Shin, C. H.; Lee, J. Y. *Progress in Zeolite and Microporous Materials*; *Studies in Surface Science and Catalysis*; Chon, H., Ihm, S.-K., Uh, Y. S., Eds.; Elsevier: Amsterdam, 1997; Vol. 105, Part A, p 45.

(21) Gregg, S. J.; Sing, K. S. W. *Adsorption, Surface Area and Porosity*; Academic Press: London, 1982.

(22) Mikhail, R. Sh.; Brunauer, S.; Bodor, E. E. *J. Coll. Interface Sci.* **1968**, *26*, 45.

(23) Lippens, B. C.; De Boer, J. H. *J. Catal.* **1965**, *4*, 319.

(24) Because there are no diffraction peaks in high 2θ range for mesoporous MCM-41, the ZSM-5 content in sample S2 can be deduced from the sum of three peak intensities in the 2θ range of 22−24°. First, mix MCM-41 with ZSM-5 phases according to various proportions such as 1/10, 1/7, or 1/5, and obtain their XRD profiles. Then, plot the sums of heights of three characteristic peaks in the range of 22−24° against the proportions of ZSM-5 to obtain a working curve. Therefore, the ZSM-5 content in sample S2 can be deduced from this working curve. Both the mechanic mixture of ZSM-5 and MCM-41 used for reference here and sample S2 have the same XRD profiles and the same Si/Al ratios.

(25) Kim, J. M.; Kwak, J. H.; Jun, S.; Ryoo, R. *J. Phys. Chem.* **1995**, *99*, 16742.

(26) Fraissard, J.; Ito, T. *Zeolites* **1988**, *8*, 350.

(27) Chen, X.; Huang, L.; Li, Q. *J. Phys. Chem. B* **1997**, *101*, 8460.

(28) Yang, P.; Zhao, D.; Margolese, D. I.; Chmelka, B. F.; Stucky, G. D. *Nature* **1998**, *395*, 152.

(29) Guo, W.; Huang, L.; Li, Q. *J. Chem. Chin. Univ.* **1999**, *20*, 3, 356.